AEPD System as a Standard On-ground Tool for Electric Propulsion Thrusters

IEPC-2017-33

Presented at the 35th International Electric Propulsion Conference
Georgia Institute of Technology • Atlanta, Georgia • USA
October 8 – 12, 2017

Fabrizio Scortecci[1] and Damiano Pagano[2],
Aerospazio Tecnologie srl, Zona Industriale Sentino, 53040 Rapolano Terme, Siena, Italy

Carsten Bundesmann [3], Christoph Eichhorn[4], Frank Scholze[5], Daniel Spemann[6]
Leibniz-Institute of Surface Modification, Permoserstr. 15, 04318 Leipzig, Germany

Hans Leiter [7]
Ariane Group, Im Langen Grund, 74239 Hardthausen-Lampoldshausen, Germany

Holger Kersten [8]
Christian-Albrechts Universität zu Kiel, Leibnizstr. 11-19, 24098 Kiel, Germany

Richard Blott [9]
Independent Consultant, Bennetts, Eastergate Lane, Chichester, West Sussex PO20 3SJ, UK

Stephane Mazouffre [10]
ICARE - CNRS, 1C Av. de la Recherche Scientifique, 45071 Orléans, France

Peter Klar [11]
Justus-Liebig Universität Gießen, Heinrich-Buff-Ring 16, 35392 Gießen, Germany

Davar Feili [12], J. Gonzales del Amo[13]
ESA-ESTEC, Keplerlaan 1, 2201 AZ Noordwijk, The Netherlands

Abstract: The European Space Agency is devoting a large effort to meet standardisation of the on-ground diagnostic tools and procedures for the qualification of the future European electric thrusters. In 2006 a first programme aimed at developing Advanced Electric Propulsion Diagnostics (AEPD) for thruster characterisation was initiated. The results of that programme lead to the development of a number of advanced diagnostics, which were successfully demonstrated on different thrusters and test facilities. Recently, a new programme aimed at improving and qualifying the AEPD system as a standard on-ground diagnostics tool for EP thruster has been performed by ESA, involving the participating institutions of the authors of this paper.

[1] Technical Manager, fscortecci@aerospazio.com
[2] Researcher, damiano.pagano@aerospazio.com
[3] Scientist, carsten.bundesmann@iom-leipzig.de
[4] Researcher, christoph.eichhorn@iom-leipzig.de
[5] Scientist, frank.scholze@iom-leipzig.de
[6] Group leader, daniel.spemann@iom-leipzig.de
[7] Team leader electric propulsion, hans.leiter@ariane.group
[8] Professor, kersten@physik.uni-kiel.de
[9] Scientist, rjb@space-enterprisepartnerships.com
[10] Scientist, Head of EP team, stephane.mazouffre@cnrs-orleans.fr
[11] Professor, Peter.J.Klar@exp1.physik.uni-giessen.de
[12] Electric Propulsion Engineer, Davar.Feili@esa.int
[13] Electric Propulsion Section Head, Jose.Gonzalez.del.Amo@esa.int

Nomenclature

d	=	electrodes separation
B	=	magnetic field
E	=	electron charge
E	=	electric field
m_i	=	ion mass
v_i	=	ion velocity
V_{acc}	=	ion acceleration voltage
V_{probe}	=	voltage difference applied to the electrodes
z_i	=	ion charge state

I. Introduction

Experimental characterization of electric propulsion (EP) thrusters or ion beam sources for material processing may provide important data both to judge their performance and to achieve a better understanding of physical processes in the plume and in the discharge chamber of such systems. Measurements of plasma parameters and monitoring of possible lifetime limiting alteration of the properties of thruster components, such as, for example, the evolution of the grid hole diameter in gridded ion thrusters, yield valuable information for the development and validation of numerical tools. Those codes, e.g. aiming at plasma and ion beam modeling (Examples: particle-in-cell code XOOPIC for charged particle and plasma simulation [7], IGUN code for simulation of ion trajectories [8]) or thruster lifetime prediction related to the erosion of ion thruster accelerator grids (Example: DynaSim code [9]), can help to partially circumvent expensive measurement campaigns with respect to thruster design and performance verification.

In this context, several groups have investigated surfaces of thruster components e.g. by telemicroscopy or thermal imaging methods [2-4,10-14]. In order to allow for the in-situ measurement of an extensive set of EP thruster performance parameters, the advanced electric propulsion diagnostic (AEPD) platform was designed and built some years ago [1,5]. The setup was modular and mobile such that it could be easily adapted to vacuum facilities of different size and experimental needs. Several measurement devices for particle beam and mechanical part characterization were implemented: a Faraday probe for thruster plume characterization, an energy-selective mass spectrometer to collect energy distribution data, a telemicroscope to measure erosion of mechanical parts, a triangular laser head to monitor the surface profile of selected parts of interest, and a pyrometer to measure surface temperature distributions. Most of the sensors consisted of commercially available devices with in-house modifications. Only the Faraday probe was manufactured completely in-house. The AEPD platform was tested successfully with two electric propulsion thrusters: a gridded ion thruster RIT-22 (Airbus Defence & Space, Germany, [1,3,4]) and a Hall effect thruster SPT-100D EM1 (EDB Fakel, Russia, [1,2]), in two different vacuum facilities.

The previous results demonstrated the capabilities of the first AEPD platform but also some limitations, mainly related to the design but also to financial needs. Therefore, a new activity has been started in order to improve the performance and availability of the diagnostic platform. At present, the activities concentrate on three major topics: (i) The setup and test of additional or alternative plasma-diagnostic tools as extension or redesign of AEPD capabilities, (ii) the implementation of partially new designs of existing sensors in order to reduce the dimension and, hence, the interaction of diagnostic head and thruster, (iii) qualification of the diagnostic platform as standard on-ground tool for EP thruster characterization.

The first aspect deals with the development and integration of new sensors in the AEPD platform, such as a retarding potential analyzer, an ExB probe or an active thermal probe [5]. The second aspect concerns rather technical issues, such as modifications related to the vacuum compatibility of some diagnostic heads, size reduction and optimization of the respective sensor housings and working distance geometries, but also the protection of the sensor heads from damage due to ion bombardment [15]. The third aspect is not addressed in this paper but will be the focus of future work, because standardization of EP diagnostics is key issue when promoting EP technologies.

In this paper, the most recent implementation of the diagnostic tools is described and first performance characterization results are presented, exemplary, for a gridded ion thruster RIT-µX (Airbus Defence & Space, [16]).

II. Experimental Set-up

A. The Multi-axis Positioning System

The AEPD platform (see Figure 1) consists of a 5-axis positioning system and several diagnostic tools. The positioning system utilizes a modular heavy bar setup, on which three ultra-high-vacuum-specified (UHV-specified) linear tables with a traveling range of 700 mm and a traveling speed of typically 30 mm/s, and two UHV-specified rotary tables are mounted. The positioning system can be easily adapted to chambers of different size. Using the linear and rotary tables, the thruster and the diagnostic heads can be positioned very precisely relative to each other, and even 1- and 2-dimensional mappings or angular-dependent measurements can be performed.

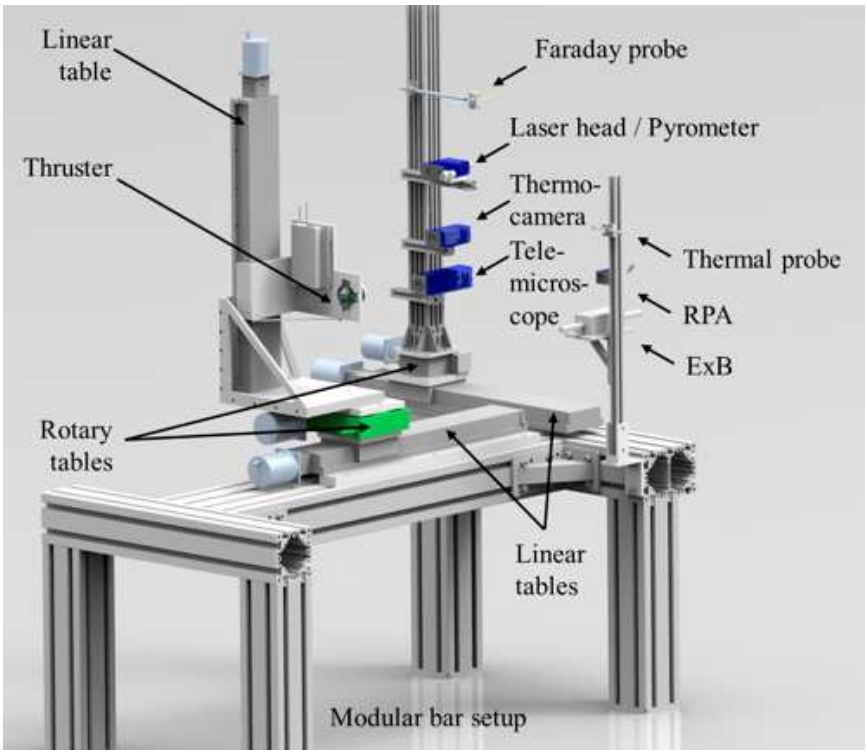

Figure 1. Drawing of the AEPD displacement system platform with modular bar frame, linear and rotary tables, thruster and a possible configuration of diagnostic tools.

At present, the AEPD platform can be equipped with diagnostic tools for beam characterization (Faraday probe, retarding potential analyzer, ExB probe, active thermal probe), optical inspection (telemicroscope, triangular laser head) and thermal characterization (pyrometer, thermocamera), which are described in more detail thereafter.

B. Faraday probe

A Faraday probe is used map the current density profile of the ion beam. Beam profiling gives access to the beam shape and its divergence.

The Faraday probe has been developed in-house [6]. It uses a graphite ion collector rod, which is embedded in a ceramic tube surrounded by a thin metal cylinder of stainless steel with a length of 101 mm and an outer diameter of 6 mm. The ion collecting diameter is as small as 1.9 mm (area 2.8 mm^2) to allow for measurements with high spatial resolution.

The ion collector is connected via a shielded BNC cable and a customized vacuum feedthrough to an external board with several high-precision resistors with different resistance. Thus, a large range of signal amplitudes can be covered. Data are recorded using a 12-bit analogue digital converter. With a sampling rate of up to 20 kHz, maximum ion current densities up to 40 mA/cm^2 with a resolution of 0.05 mA/cm^2 can be detected.

C. Retarding Potential Analyser

A retarding potential analyzer is used to measure the energy distribution of charged particle, i.e. ions. It is based on measuring the ion current in dependence on the repelling voltage (electrostatic energy analyzer).

The retarding potential analyzer was also developed in-house with the goal to make it as small as possible while keeping the performance (signal-to-noise ratio) sufficiently high. Therefore, a grid design with 149 holes has been chosen. The device consists of two grids and an ion collector. The first grid is used for focusing the ion trajectories, the second grid for repelling secondary electrons. The ion collector is used for measuring the ion current and for repelling the ions by applying a repelling voltage. The holes of the first grid have a diameter of 0.4 mm. The first grid could also be used for measuring the ion current density. The measurement area is 24 x 24 mm^2. The ion collector has cup-shaped cavities, one for each of the 149 ion channels. The repelling voltage can be varied between 0 V and 3000 V with accuracy better than 0.05 %. The collected ion current is transformed by a high-precision resistor into a voltage drop, which is measured by a 14-bit AD converter. The accuracy is better than 5 eV. The overall dimension of the device is 40 x 47 x 84 mm^3.

D. ExB Probe

The ExB probe exploits the action of a magnetic (B) and an electric field (E) to select ions on the basis of their velocity v_i: only ions whose velocity satisfies the Wien condition (Equation 1) are able to pass through the filter and thus being detected [17]. d is the distance between the fixed electrodes, where the electric field is created.

$$v_i = \frac{E}{B} = \frac{V_{probe}}{B \cdot d} \quad (1)$$

Because the velocity is a function of charge state z_i, mass m_i and ion energy $E_{ion,i}$, different ion species can be separated. Equation 2 expresses the electrodes' voltage difference associated with each peak in the spectrum:

$$V_{probe} = B \cdot d \cdot \sqrt{\frac{2 \cdot z_i \cdot E_{ion,i}}{m_i}} \quad (2)$$

On one hand a constant magnetic field is used to deflect ions' trajectories, on the other hand a variable electric field acts for compensating the magnetic force, which allows ions with different velocity to be detected as a function of the voltage applied to electrodes. While in retarding potential analyzer measurements the voltage ramp to be applied to the retarding grid is directly connected to the accelerating voltage of the thruster, in case of the ExB probe the voltage range to be scanned depends also on the constructive parameters of the probe (magnetic field intensity, electrodes separation). These constructive parameters affect the performances of the probe in terms of resolution.

The main aim was to develop a probe, which is able to put together high performances with low invasiveness. These aspects can be considered conflicting because an increase of the probe resolution can be determined by an increase of the magnetic field, and an increase of the magnetic field is usually associated with larger magnets. This problem was overcome by exploiting a particular magnetic configuration known as Stelter dipole allowing a significant increase of the magnetic field with respect to a "traditional" dipole with the same overall dimension. In particular, a maximum field of 0.54 T has been obtained for a probe having a 50 x 50 mm^2 section.

Another important aspect taken into account in the probe design concerns the topology of the magnetic and electric fields at the entrance and the exit of the probe. The different decaying behavior of the fields makes the probe not ideal, thus the Wien condition is no more satisfied in these regions. To overcome this problem the electrodes' shape has been optimized in order to make the electric fringing field matching the magnetic one.

The spatial resolution of the probe is determined by two collimators at the entrance and exit of the probe selecting ions traveling along a well-defined direction. A modular design approach has been implemented allowing to easily changing the collimator length and the orifice diameter.

The probe is mainly used to determine the plasma composition in terms of ion species fraction because of the dependence of the ion velocity on the charge state. Assuming that all ion species are subject to the same accelerating voltage, the separation between the peaks' position will be given by the square root of the different charges over their masses . The area under each peak yields the current carried by each ion species. Therefore, the ratio between this area and the area under the overall spectrum provides the current fraction (neglecting secondary emission effects). On the other hand the position of each peak is connected with the ion velocity through the constructive parameters of the probe: in particular the ion velocity distribution function for each ion species could be determined. This application requires a calibration of the probe providing a correction factor to be applied to the measured ion velocity to obtain the real one.

The ExB probe is an in-house development. The entrance orifice diameter is 1.6 mm, the length off the entrance collimator is 90 mm, and the Wien filter length 150 mm. The overall dimension is 50 x 50 x 280 mm^3. Velocities up to 100000 m/s with a resolution of about 1000 m/s can be measured.

E. Active Thermal Probe

The active thermal probe (see Figure 2) was developed during a previous project as a flexible diagnostic for the measurement of energy flux. For the use as a diagnostic tool for beam characterization as a part of the AEPD platform, it has been further improved and characterized especially regarding it´s sensitivity towards parasite heat sources.

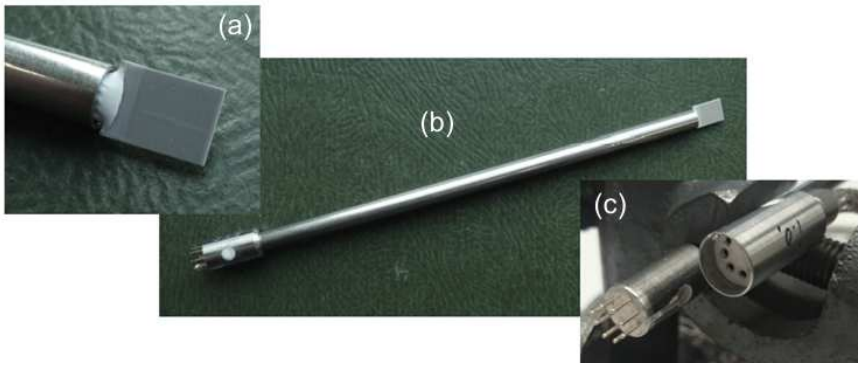

Figure 2 – Active thermal probe: Sensor area (a), full image (b) and connector (c).

The physical principle of the measurement method of the active thermal probe is based on the compensation of the incoming energy by decreasing the heating power of a preheated probe. The probe consists of a ceramic dummy-substrate (see Figure 2 (a)), which is electrically heated to a given set-point temperature. If the probe is exposed to an external energy flux (e.g. by the ion beam) the additional heating of the probe is compensated by a reduction of the electrical heating power, resulting in a constant temperature of the probe. The power of the external energy source is then directly given by the difference in the electrical heating power. In contrast to the other probes, the ATP measures both the contribution of charged and neutral particles. A much more detailed description of the working principle of the active thermal probe can be found in Refs. [18,19,20].
The measurement range is between 1 x 10^{-3} W/cm^2 and 4 W/cm^2 with a sensitivity of ± 1 x 10^{-3} W/cm^2. The sensor dimension is 7 x 10 x 0.3 mm^3.

F. Telemicroscope

The telemicroscope is a high-resolution optical camera, which can be used to image mechanical parts. The images can be used to measure radial (or axial upon exploitation of the reduced depth of field) erosion.
The telemicroscope consists of a CCD camera, an extension tube and a photographic lens. By placing the extension tube between camera and lens, the radial resolution and depth of field is reduced considerably. All parts are commercially available (The Imaging Source). The setup has changed slightly compared to the previous one [1]. Now a smaller lens and a camera with a higher resolution is used, which results in a smaller overall dimension and a better performance.
The telemicroscope is now operated inside vacuum. Therefore, some vacuum-sensitive electronic parts (capacitors) had to be replaced. For safety reasons the device is covered by a small housing, which consists of a metal base plate, a front plate made of graphite with sapphire window and a metal cover. The window protects the optics from direct particle impingement. Additionally, the telemicroscope housing is equipped with four high-power LEDs for illumination.
The lens has a focal length of 50 mm and an extensions tube with a length of 40 mm is used. The resolution of the CCD camera is 1600 pixel x 1200 pixel. The overall dimension (including housing) is 60 x 70 x 210 mm^3
Figure 3 shows a graticule test structure, which was used for performance evaluation. The image size (field of view) is 8.75 x 6.56 mm^2 at a working distance of 112.5 mm. The radial accuracy is better than 0.01 mm. The depth of field (axial resolution) is better than 0.5 mm.

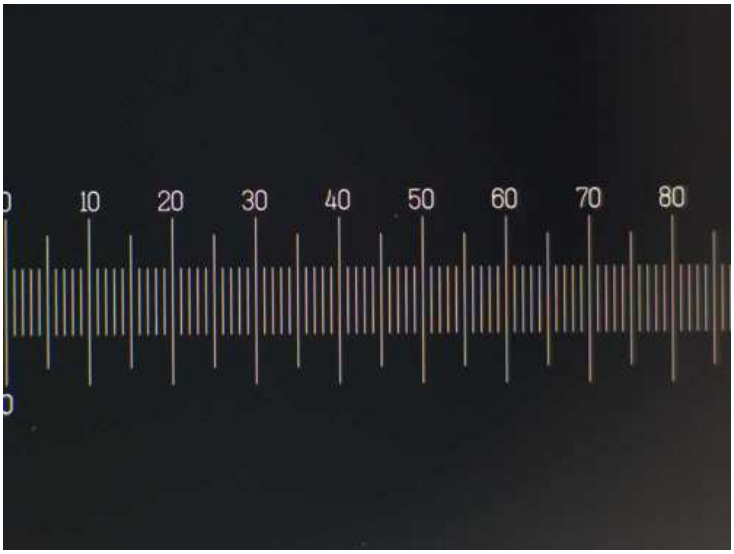

Figure 3. Telemicroscope image of an eyepiece graticule test structure.

G. Triangular Laser Head

The triangular laser head is used to measure surface profiles, which gives access to axial (and radial) erosion or surface deformation, e.g. grid curvature of gridded ion engines, of mechanical parts.

The triangular laser head measures the distance to a test object utilizing the triangulation principle, i.e. the fact that the detection angle α depends on the distance between triangular laser head and test object (see Figure 4). When scanning across the test object, the surface profile can be measured, which gives access to axial (and radial) erosion.

The triangular laser head (Keyence LK-G152) is commercial devices. The triangular laser head is the same one that was used with the previous setup [1]. The triangular laser head is also operated inside vacuum. Again, some vacuum-sensitive electronic parts (capacitors) had to be replaced. The triangular laser head is also placed in a small housing, which is similar to the one of the telemicroscope.

The distance range covers 110 mm - 190 mm with a specified repeatability of < 0.001 mm and distance resolution of < 0.01 mm. The spot size is about 0.2 mm at a distance of 150 mm. The overall dimension of the device (including vacuum housing) is 95 x 47 x 127 mm^3.

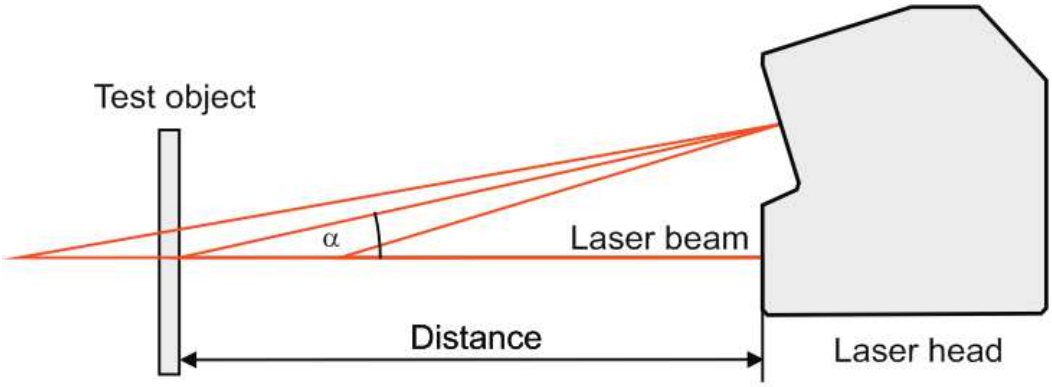

Figure 4. Measurement principle of the triangular laser head (triangulation effect).

H. Thermocamera

A thermocamera is used in order to image the surface temperature of mechanical parts of interest upon detection of the emitted infrared radiation. The physical principles are described by Planck's law, i.e. the intensity of the emitted infrared radiation is proportional to the surface temperature. When measuring the temperature, the properties of the test object, i.e. the emissivity of the material of interest, and of the setup, i.e. window effects, must be considered.

The thermocamera (Optris PI) is a commercial device. It was chosen because of its small size, which reduces possible interactions with the energetic particle beam. The thermocamera is operated inside vacuum. Again, some vacuum-sensitive electronic parts (capacitors) had to be replaced. The thermocamera is surrounded by a metal housing (with a ZnS window) for safety reasons [15]. The housing is similar to that of the telemicroscope. The overall dimension of the thermocamera (including housing) is 56 x 60 x 143 mm^3

The thermocamera operates in the spectral range from 7.5 µm to 13 µm. The image size is about 0.05 m x 0.07 m at a working distance of 500 mm. The resolution of the camera is 160 pixel x 120 pixel. The lateral resolution is 1.5 mm. Temperature range and resolution is specified to be 0°C – 900°C and 0.1°C, respectively. The system accuracy is given to be 2 % of reading or 2°C.

the advantage that they can be brought closer to the test object. A smaller working distance results in Operating the diagnostic heads inside vacuum has a better lateral resolution, which is especially favorable for the thermocamera.

I. Pyrometer

The Pyrometer operation is based on the same principle as the thermocamera i.e. Planck's law. In contrast to the thermocamera, the pyrometer can perform temperature spot measurements.

The pyrometer (Optris CT 3M) is a commercial device. It is different to the one, which was used in the previous setup [1,4]. The new device is much smaller than the previous one. The new pyrometer is now operated inside vacuum. Therefore, some vacuum-sensitive electronic parts (capacitors) had to be replaced or removed (liquid crystal display). The sensor head is placed inside a metal housing with a sapphire [15]. The overall dimension (including housing) is 25 x 30 x 47 mm^3.

The pyrometer operates at a wavelength of 2.3 µm. The spot size is 1.5 mm at the focal distance of 110 mm. Temperature range and resolution are 150°C – 1000°C and 0.1°C, respectively. The system accuracy and repeatability are given to be 0.3 % of reading + 2°C or 0.1 % of reading + 1°C.

III. Selected Results

Tests were carried out on two different thrusters, the RIT-µX [15] supplied by Ariane-Group and a SPT-100 ML supplied by ICARE-CNRS. Test were performed in two different test facilities, the Jumbo facility at the University of Giessen and the Medium Vacuum Test Facility No.1 in AEROPSAZIO Tecnologie.

Data are presented here for the test performed at the University of Giessen on the RIT-µX . The thruster was operated here at two reference operation points (OP1=1050V/ 4mA, and OP2=1700V/ 8mA).

A. Faraday Probe

Selected current density maps are plotted in Figure 5. As expected, rotationally symmetric, Gaussian shaped beam profiles can be seen with a higher maximum current density at operation point 2 (j_{max} = 0.52 mA/cm^2) than at operation point 1 (j_{max} = 0.18 mA/cm^2). This is related to the higher beam voltage at operation point 2. The full width at half maximum of the beam profiles is very similar for the two operation points (OP1: 48.0 mm; OP2: 40.8 mm).

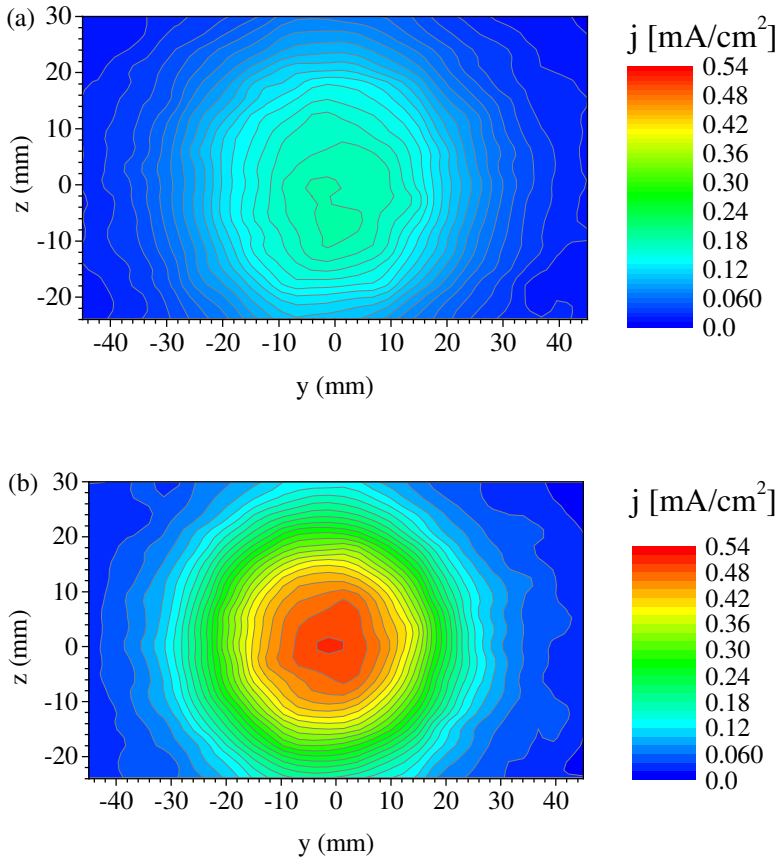

Figure 5. Current density maps of the RIT-µX at OP1 (a) and OP2 (b) measured with the Faraday probe at a distance of 120 mm to the exit plane.

B. Retarding Potential Analyser

The energy distribution of the extracted ions was measured at the two operation points, too. Figure 6shows, exemplary, the result for operation point 1. The energy distribution reveals a single peak. The peak position is close to the beam voltage, which is the main contribution to the ion energy. However, the plasma potential and the secondary star ground have also in impact on the measurement result. The width at half maximum of the peak is smaller than 20 V, which corresponds to less than 2 % of the ion energy. Ions with other energies, which could be generated by charge exchange processes, or multiply charged ions were not detected.

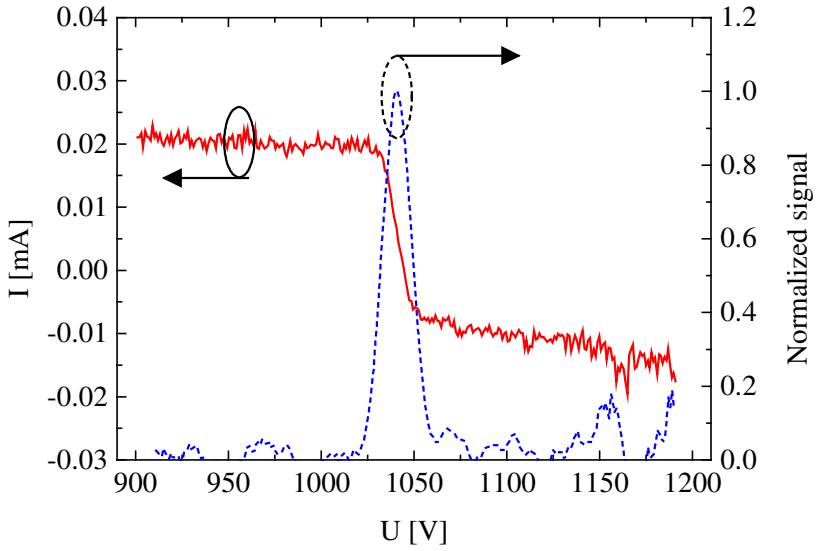

Figure 6. Current signal (solid curve) measured with the retarding potential analyzer and calculated energy distribution (dashed curve) of the extracted ions, exemplary, for OP1.

C. ExB Probe

Ion velocity measurements were performed with the ExB probe positioned along the thruster axis at a distance of 350 mm from the thruster exit plane. Figure 7 shows two spectra obtained for the two operation points of the thruster. The position of the peaks corresponds to the different ion velocity, which is proportional to the square root of the ion energy. The most pronounced peaks at an electrode voltage difference of ~ 87 eV (OP1) and ~ 111 eV (OP2) can be assigned to singly charged ions (Xe^{+}). As expected, the ratio of the peak positions is (approximately) the same as the square root of the ratio of the corresponding beam voltages. In the curve for operation point 2 a second peak at an electrode difference voltage of ~ 153 eV can be seen. This peak is related to doubly charged ions (Xe^{2+}). The peak is very small, i.e. the fraction of doubly charged ions is low, as it is typical for gridded ion thrusters.

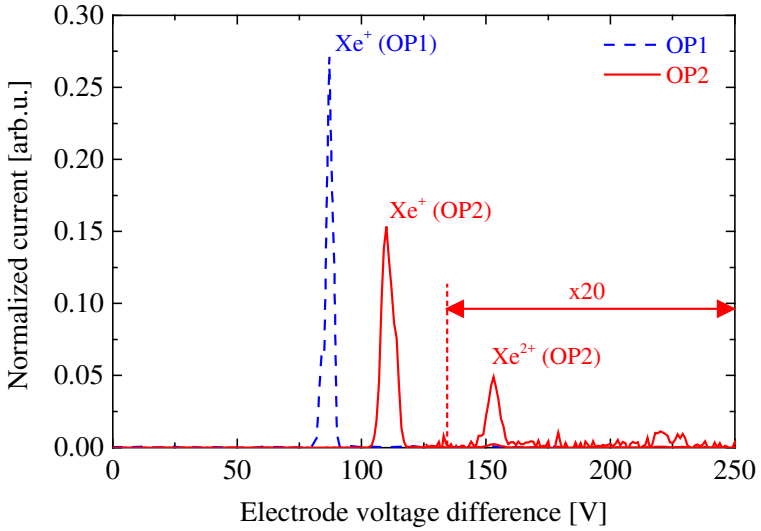

Figure 7. ExB probe normalized spectra at OP1 (dashed curve) and OP2 (solid curve) at a distance of 350 mm to the exit plane of the thruster.

D. Active Thermal Probe

In Figure 8 selected results for the measurement of the energy flux density under variation of the vertical position relative to the center axis of the thruster are presented.

The thruster was aligned in such a way that the beam hits the probe at normal incidence and that the center of the thruster grid has a distance of 490 mm to the probe. Figure 8 summarizes the results of two measurements for the two thruster operation points each. The data illustrate clearly that the measurements show a good reproducibility and give access to the radial distribution of the energy flux density of the beam. Furthermore, it should be pointed out that even close to its lower detection limit of 1 mW/cm^2 the probe gives reproducible results.

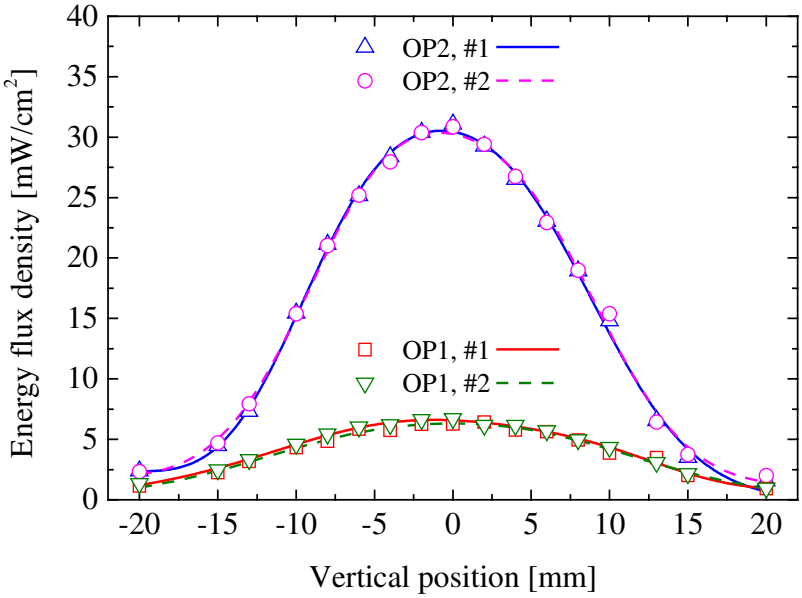

Figure 8. Energy flux density vs. vertical position for the RIT-µX running at OP1 and OP2 measured with the active thermal probe. The symbols represent the experimental data; the solid lines give cubic spline interpolations. There are two measurements for each operation point.

E. Telemicroscope

Figure 9 shows a section of the grid of the thruster (thruster is off). The grid holes can be clearly resolved and grid hole diameter and, hence, the grid hole erosion are accessible. The diameter of the center hole in Figure 9 is (1.27 ± 0.02) mm.

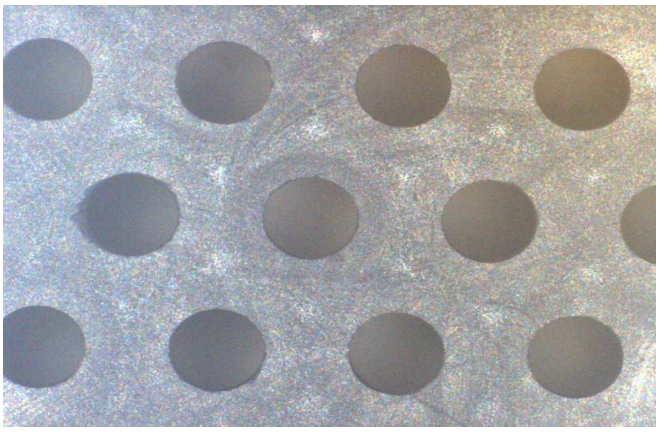

Figure 9. Telemicroscope image of grid holes of the RIT-µX.

F. Triangular Laser Head

Figure 10 shows a surface profile scan of the thruster. Among others, the grid hole area can be identified clearly and the number of holes can be seen. Doing so, the principal shape of the grid including, for instance, its radius of curvature could be measured [3,4]. In case of the RIT-µX the grid is flat. However, there are experimental limitations due to the measurement principle (triangulation effect). Because of that, the triangular laser head might fail in measuring the profile at steep or abrupt edges (see details in Figure 10).

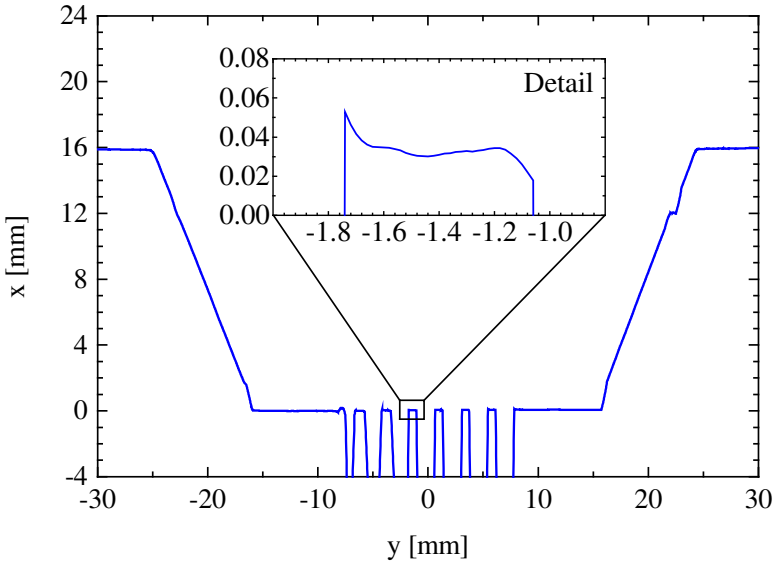

Figure 10. Surface profile scan across the center of the RIT-µX measured with the triangular laser head. The detail inset shows the measured surface profile scan between two grid holes. The rise of the profile at the left side is a measurement artifact due the triangulation measurement principle.

G. Thermocamera

Figure 11 (a) shows a thermocamera image of the RIT-µX operated at operation point 2. The surface temperature of almost the whole thruster is imaged. The temperature distribution is nearly homogeneous, apart from the holes. As shown in previous tests, the temperature of the plasma chamber, which is imaged through the holes is considerably higher than the grid surface temperature [3,4]. In Figure 11 (b) two temperature line scans, which were extracted from thermocamera image, are plotted. The grid temperature was found to be (68°± 2)°C.

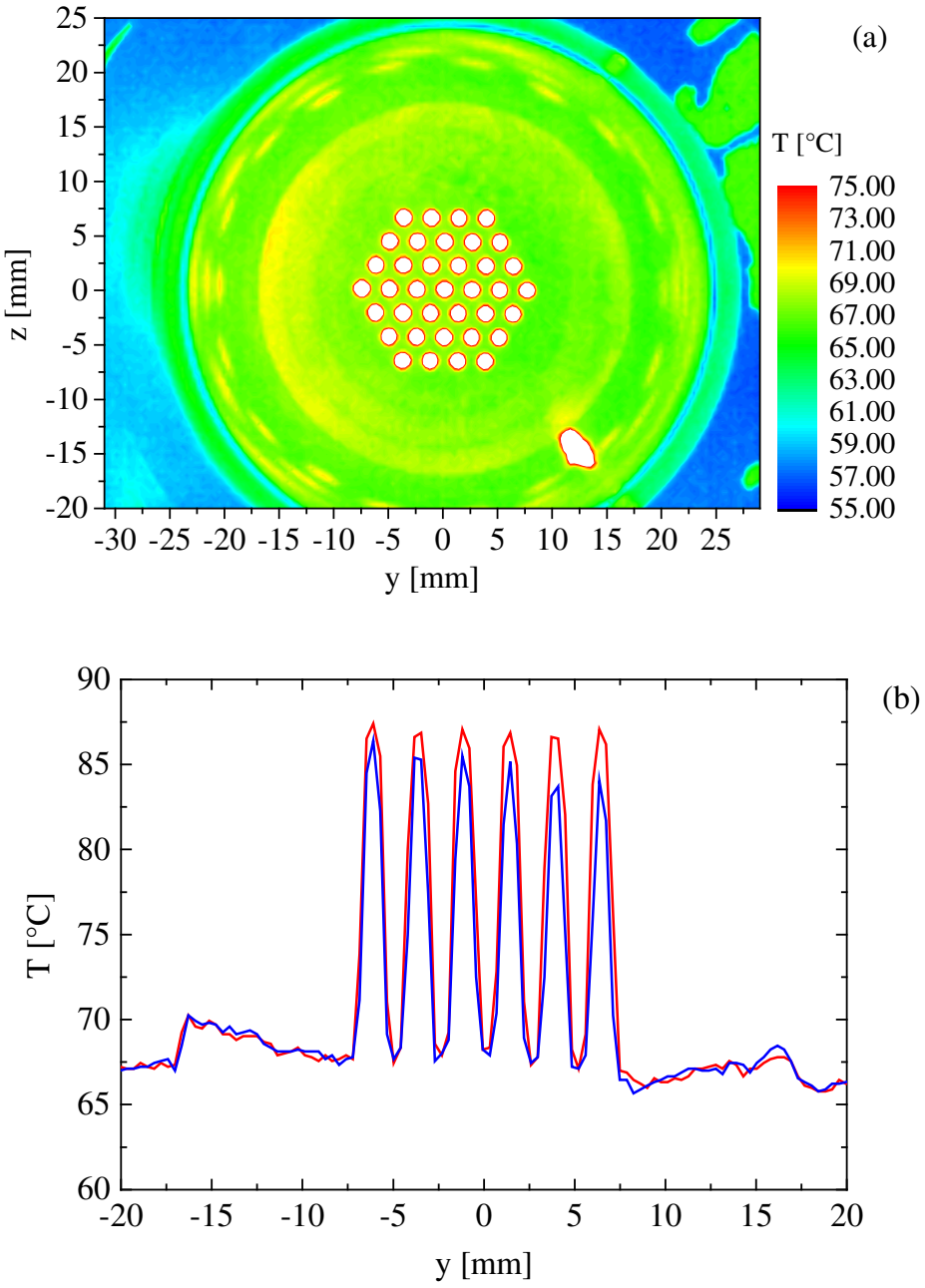

Figure 11. (a) Thermocamera image of the RIT-µX at OP2. (b) Horizontal temperature scans across the center of the thruster extracted from thermocamera image in panel (a).

IV. Conclusion

The experimental data demonstrate impressively the capabilities of the AEPD platform, which allows a comprehensive characterization of electric propulsion thrusters or ion beam sources for material processing.
Typically, the main focus lies on investigating beam properties, because the beam provides the thrust or, in material science, the tool for material modification. Important parameters are particle energy or velocity, beam shape and divergence, composition, charge state. All of these parameters can be measured with the current setup. It is not only possible to measure the properties of charged particles (Faraday probe, retarding potential analyzer, ExB probe) but also of energetic neutrals (active thermal probe).
The optical inspection tools (triangular laser head, telemicroscope) provide important information about the shape of mechanical parts and its evolution in time (erosion), which can be life-limiting factors. The triangular laser head is advantageous when measuring axial dimensions, whereas the telemicroscope has its advantage when measuring radial dimensions. However, both devices can be used to measure axial and radial dimensions, though with different accuracy.
Thermal characterization is important, for instance, for evaluating the thermal impact on the performance of satellites (in case of electric propulsion thrusters). Both pyrometer and thermocamera provide similar information. In case of small thrusters, the thermocamera can yield a full thermal image. In case of larger thrusters (with higher power), scanning with the pyrometer seems to be more appropriate due to its smaller dimension.
We have reported about improvements of our AEPD platform. The activities are focused on modifying the experimental setup in order to reduce possible interactions between diagnostics and thruster, on implementing additional or alternative diagnostic heads in order to improve the performance or to expand the portfolio of accessible parameters. We have described the main parameters of the new diagnostic tools and presented first experimental results, exemplary, with a gridded ion thruster RIT-μX.
It can be stated that the improvements on the AEPD platform have improved reliability and repeatability, and, therefore, constitute a major step towards standardization, which is intended to be the final goal. In order to reach this goal, significant effort is still necessary to provide suitable standards.

Acknowledgments

The AEPD-2 activity was carried-out for the European Space Research and Technology Centre of ESA within project 4000107451/12/NL/RA.

References

[1] C. Bundesmann, M. Tartz, F. Scholze, H.J. Leiter, F. Scortecci, R.Y. Gnizdor, H. Neumann, Rev. Sci. Instrum. **81** (2010) 046106.

[2] C. Bundesmann, M. Tartz, F. Scholze, H. Neumann, F. Scortecci, S. Scaranzin, P.−E. Frigot, J. Gonzalez del Amo, R.Y. Gnizdor, in *Proc. of the 31st Int. Electric Propulsion Conf., Ann Arbor, 2009*, Paper IEPC-2009-141.

[3] C. Bundesmann, M. Tartz, F. Scholze, H. Neumann, H.J. Leiter, F. Scortecci, D. Feili, P.−E. Frigot, J. Gonzalez del Amo, in *Proc. of the 31st Int. Electric Propulsion Conf., Ann Arbor, 2009*, Paper IEPC-2009-160.

[4] C. Bundesmann, M. Tartz, F. Scholze, H. Neumann, H.J. Leiter, F. Scortecci, J. Propul. Power **27** (2011) 532.

[5] D. Pagano, F. Scortecci, C. Bundesmann, C. Eichhorn, F. Scholze, H. Neumann, H. Leiter, H. Kersten, S. Gauter, R. Wiese, R. Blott, P.J. Klar, K. Holste, B. Meyer, S. Mazouffre, A. Bulit, J. Gonzales del Amo, in *Proc. of the 34th Int. Electric Propulsion Conf., Hyogo-Kobe, 2015*, Paper IEPC-2015-363.

[6] C. Eichhorn, F. Scholze, C. Bundesmann, H. Neumann, in *Proc. of the 33rd Int. Electric Propulsion Conf., Washington, 2013*, Paper IEPC-2013-295.

[7] J.P. Verboncoeur, A.B. Langdon, N.T. Gladd, Comp. Phys. Comm. **87** (1995) 199.

[8] R. Becker and W. B. Herrmannsfeldt, Rev. Sci. Instrum. **63** (1992) 2756.

[9] M. Tartz, E. Hartmann, H. Neumann, Rev. Sci. Instrum. **79** (2008) 02B905.

[10] M. Crofton, R. Ueunten, L. Harris, E. Yohnsee, R. Cohen, in *Proc. of the 32nd AIAA Joint Propulsion Conf. and Exhibit, Lake Buena Vista, 1996*, Paper AIAA-96-2977.

[11] S. Mazouffre, P. Echegut, M. Dudeck, Plasma Sources Sci. Technol. **16** (2007) 13.

[12] S. Mazouffre, K. Dannenmayer, J. Pérez-Luna, J. Appl. Phys. **102** (2007) 023304.
[13] T. Misuri, A. Milani, M. Andrenucci, in *Proc. of the 31st Int. Electric Propulsion Conf., Ann Arbor, 2009*, Paper IEPC-2009-036.
[14] T. Misuri, T. Vrebosch, L. Pieri, M. Andrenucci, M. Tordi, E. Marcuzzi, M. Batolozzi, S. Renzetti, J. Gonzalez del Amo, in *Proc. of the 32nd Int. Electric Propulsion Conf., Wiesbaden, 2011*, Paper IEPC-2011-129.
[15] C. Bundesmann, C. Eichhorn, F. Scholze, H. Neumann, H.J. Leiter, F. Scortecci, in *Proc. of the 34th Int. Electric Propulsion Conf., Hyogo-Kobe, 2015*, Paper IEPC-2015-392.
[16] C. Altmann, H. Leiter, R. Kukies, in *Proc. of the 34th Int. Electric Propulsion Conf., Hyogo-Kobe, 2015*, Paper IEPC-2015-274.
[17] D. Renaud, D. Gerst, S. Mazouffre, A. Aanesland, Rev. Sci. Instrum. **86** (2015) 123507.
[18] R. Wiese, Dissertation, Ernst-Moritz-Arndt Universität, Greifswald, 2008.
[19] R. Wiese, H. Kersten, G. Wiese, M. Häckel, Vakuum in Forschung und Praxis **23** (2011) 20.
[20] R. Wiese, H. Kersten, G. Wiese, R. Bartsch, EPJ Techniques and Instrumentation **2** (2015) 2.
[21] P.J. Klar, K. Hannemann, U. Ricklefs, H. Leiter, in *Proc. of the 34th Int. Electric Propulsion Conf., Hyogo-Kobe, 2015*, Paper IEPC-2015-89.